A mineralogical inventory of geothermal features southeast of the Salton Sea, Imperial County, California

Paul M. Adams and David K. Lynch

The Aerospace Corporation, P. O. Box 92957, Los Angeles, CA 90009

Introduction

The Salton Trough is a topographic low in southern California and northern Baja and Sonora Mexico that represents the transition between the San Andreas Fault system and rifting centers in the Gulf of California. The area is seismically active and has a high geothermal gradient that supports a number of commercial geothermal electricity generating plants. The heat from the geothermal field is the result of a shallow magma body from one or more spreading centers. The Salton Sea occupies the lowest part of the Salton trough in Imperial County, CA.

The purpose of this paper is to document the surface mineralogy of the Salton Sea geothermal features, with particular attention to those minerals not included in Pembertons' Mineralogy of California (1983). The three areas to be described range from 1) a high temperature very active ammonia-emitting and sulfate-rich fumarole area which has an unusual assemblage of ammonium sulfate minerals, 2) a moderately active geothermal fumarole area with minor ammonia-free sulfate mineralization, and 3) a carbonate-rich sulfate-poor cold mound spring system.

The high temperature fumarole area has been studied by long wavelength infrared (LWIR) hyperspectral remote sensing using the SEBASS and Mako sensors (Hackwell, et al., 1996, Warren, et al., 2010) which have identified ammonia emissions (Tratt, et al., 2011). Mineral identifications reported in this paper will be used in ongoing remote sensing efforts to map mineral distributions associated with these geothermal features.

Mineral identifications were made using powder X-ray diffraction (XRD), coupled with energy dispersive X-ray spectroscopy in the scanning electron microscope (SEM). Fourier transform infrared (FTIR) spectroscopy was performed in the field with an Agilent/A2 Exoscan portable spectrometer for comparison with remote sensing measurements.

F1–F2 Fumarole Field mineralogy

The F1 and F2 fumarole fields are located on a sand spit east of what was Mullet Island (see this volume), 5 miles SW of Niland, and have been described in detail by Lynch, et al. (2013). During their initial survey several unusual ammonium sulfates were identified, including boussingaultite and lecontite. More detailed follow on field studies were conducted during October 2013–January 2014. F1, the westernmost fumarole field, is elliptical, about 25 m x 50 m, and has abundant small clear boiling pools, sulfur vents and associated sulfate crusts and accumulations (Figure 1). The subsurface generally consists of dark gray to black mud, sand and locally has hard deposits of cemented small pelecypod shells. Living plants are in close proximity to the fumaroles and dead plant material is common and often mixed in with the mud and ammonium salts. Water and mud temperatures range from ambient to boiling. The F2 field is roughly 120 m x 400 m and irregular in shape. It is subdivided into the F2 north complex (F2NC), a small outlier to the northwest and the F2 base complex (F2BC). The fluids at F2 are more viscous than at F1 which has allowed the development of mud pots and mud volcanoes/gryphons to 1–2 m high (Figure 2), though the height varies with time and seasonal ground water levels.

The mineralogies of F1 and F2 are similar and ammonium sulfates are present at both fields. Sulfur vents and living and dead vegetation are more common at F1, compared with F2. The fumaroles at F1 are less extensive and more approachable than F2. Plumes of ammonia gas have been observed emerging from the F1 and F2 fields (Tratt, et al. 2011) and are thought to produce the ammonium sulfates. The source of the ammonia has been assumed to be from thermal decomposition

of fertilizer residues from agricultural runoff or decomposing plant matter. However, it is noted that elevated levels of dissolved ammonia have been measured in the deep seated hypersaline brines beneath the region (McKibben, 2008). Ammonium sulfates have been found at other fumarole fields where irrigation and agricultural runoff are not a potential source of ammonia. This includes ammonioalunite, ammoniojarosite, boussingaultite, letovicite, mascagnite, and tschermigite from the Geysers in Sonoma County, CA (Dunning and Cooper, 1993; Koenig, 1969) and boussingaultite from Coso Hot Springs Inyo County CA (Anthony, et al., 2003; Ross and Yates, 1942).

The pH of the water in the bubbling and boiling pools (measured with colorpHast pH strips) is nominally neutral (6.5–7.5) and the total dissolved solids in 4 clear to milky pools range from 0.3 to 8.7 wt %. Residues remaining after evaporation consist primarily of halite though gypsum was the main constituent of two pools (Table 1). Minor to trace amounts of ammonium salts, such as sal ammoniac, lecontite and boussingaultite occur in some residues. As a result, it is clear that the extensive ammonium sulfate salts do not form from the simple evaporation of the water from the bubbling and boiling pools. Instead it is conjectured that ammonia and SO_2/H_2S percolating through the wet sand and mud near gas vents react to form ammonium sulfate solutions that are concentrated and then brought to the surface by capillary action to form the efflorescent growths (Figure 3).

As a result of this study four new minerals (lecontite, koktaite, tamarugite and konyaite) have been identified that previously had not been reported from California (Pemberton, 1983). Based on preliminary remote sensing

Figure 1. Clear boiling pool (20 cm) with mascagnite, gypsum, lecontite and boussingaultite salt crusts. F1 fumarole field.

Figure 2. Small gryphon (1 m) "Sulfur Hill" with nitratine, mascagnite, boussingaultite efflorescence. F2 fumarole field.

Figure 3. Ammonium sulfate mineralization (2 m x 3 m) around a small bubbling pool and vent. Southeast F2 fumarole field. White areas contain mascagnite, with thin (1 ft) outer rim of boussingaultite. Dark brown outer ring contains nitratine.

Table 1. Total dissolved solids (TDS, wt%) from water sources and mineralogy of solid residues after evaporation. XXXX = Major, Xxxx = Minor, xxxx = trace constituent.

Location	Sample	TDS (wt%)	Residue Determined by XRD
F1	A	0.3	GYPSUM, Halite, Sal ammoniac, lecontite, boussingaultite
F1	B	0.3	HALITE, Gypsum, lecontite, boussingaultite, sal ammoniac
F2	WP303	0.3	HALITE, Sal ammoniac, Gypsum, lecontite
F2	WP450	0.3	GYPSUM, Mascagnite, boussingaultite, lecontite
F2	WP451	3.4	HALITE, gypsum, sal ammoniac, sylvine, calcite?
F2	N Pool	8.7	HALITE, gypsum, unknown?
F2	SE Pool	0.3	HALITE, Gypsum, Sal ammoniac, boussingaultite
Rt 111	S1	2.0	HALITE, dolomite, magnesite
Rt 111	S2	1.9	HALITE, sylvine, dolomite, magnesite
Rt 111	S6	2.0	HALITE, dolomite, magnesite, sylvine
Salton Sea		4.8	HALITE, gypsum, bloedite, hexahydrite

studies the F1 fumarole field appears to have much more extensive nitratine deposits and less gypsum–bloedite–thenardite than F2, though locally the mineralogies are very similar.

Sulfur S

Dry hissing thermal vents up to 3 cm in diameter commonly have intergrowths of yellow bladed sulfur crystals associated with them (Figure 4). Dendritic growths of sulfur crystals have also been seen growing on dead vegetation. These vents are at ground level at F1 but at F2 they may also be near the summits, or on the flanks, of gryphons. The individual crystals range up to 3 mm in length and have a skeletal appearance (Figure 5). Beneath the surface, close to the vents, cavities (to 8 cm) in wet black mud often have a thin lining of sulfur. Crude bladed gypsum crystals (to 0.5 mm) are often associated

with, or in close proximity, to the sulfur crystals. Sulfur crystals associated with these fumarole vents had been documented by Hanks (1882) as early as the late 1800's.

Gypsum $CaSO_4 \cdot 2H_2O$

Mats of white to cream-colored crude bladed gypsum crystals (to 1 mm) are often associated with sulfur vents and mascagnite (Figure 6). Gypsum may also occur as fibrous aggregates and clear thin fibers found underneath other sulfate crusts. Other associated species include boussingaulite, tschermigite and koktaite.

Mascagnite $(NH_4)_2SO_4$

White, cream or light gray botryoidal crusts of mascagnite (to 10 cm) are relatively common and are often found close to sulfur vents and boiling pools at both F1 and F2. The mascagnite is typically very

Figure 4. Dendritic sulfur crystals surrounding a gas vent (1 x 1.5 cm opening). F1 fumarole field.
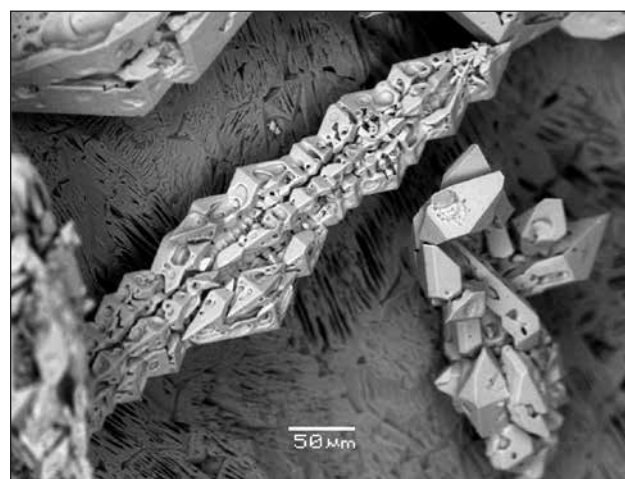

Figure 5. Cavernous sulfur crystals in parallel growth from F1 fumarole field. SEM image.
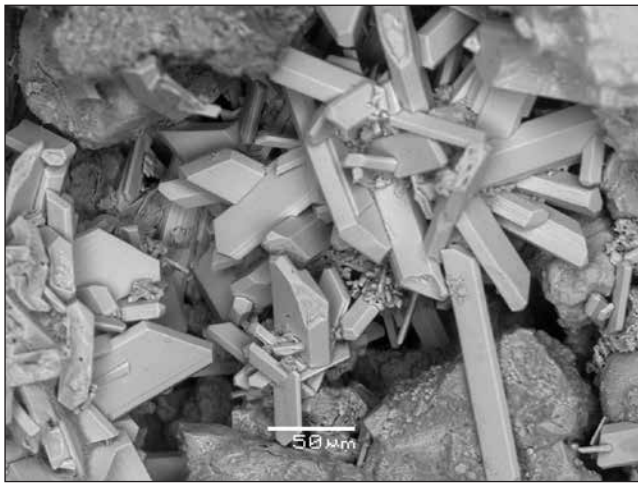
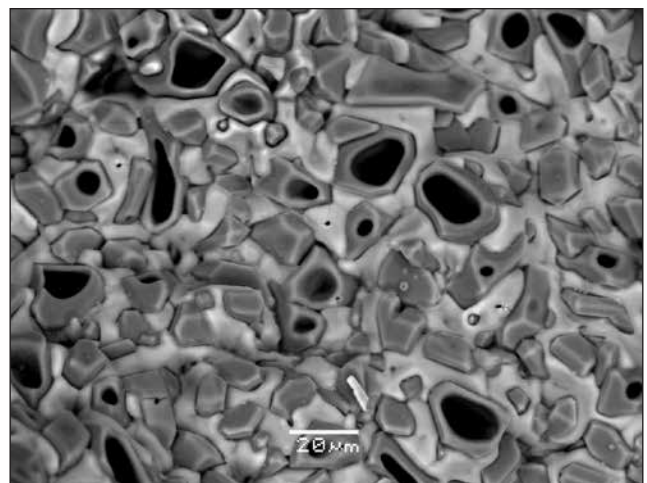Figure 6. Gypsum crystals from F1 fumarole field. SEM image.

Figure 7. Sal ammoniac (light gray) between cavernous mascagnite crystals. SEM image.
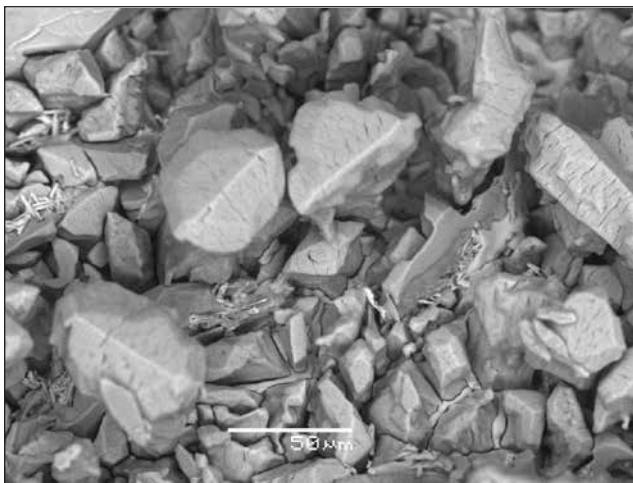

Figure 8. Lecontite crystals from F2 fumarole field. SEM image.

Lecontite (NH$_4$,K)Na(SO$_4$)·2H$_2$O

Botryoidal mascagnite crusts from F1 and F2 occasionally contain minor amounts of lecontite. It also occurs with boussingaultite at F2. Euhedral lecontite crystals (to 0.1 mm) have only been recognized in a few specimens of more pure lecontite from F1 (Figure 8).

Koktaite (NH$_4$)$_2$Ca(SO$_4$)·2H$_2$O

Minor amounts of koktaite have been identified with boussingaultite and mascagnite by XRD in samples from F1 and F2. It has not been recognized in hand specimens.

Boussingaultite (NH$_4$)$_2$Mg(SO$_4$)$_2$·6H$_2$O

Boussingaultite is often a constituent of botryoidal crusts associated with vents. It commonly occurs with mascagnite, lecontite, tschermigite, koktaite and bloedite. Crystals are typically only a few tenths of a mm long but larger corroded bladed crystals (to

fine grained but bladed crystals to 0.2 mm have been observed. Mascagnite may also be associated with lecontite, boussingaultite, koktaite or sal ammoniac (Figure 7).
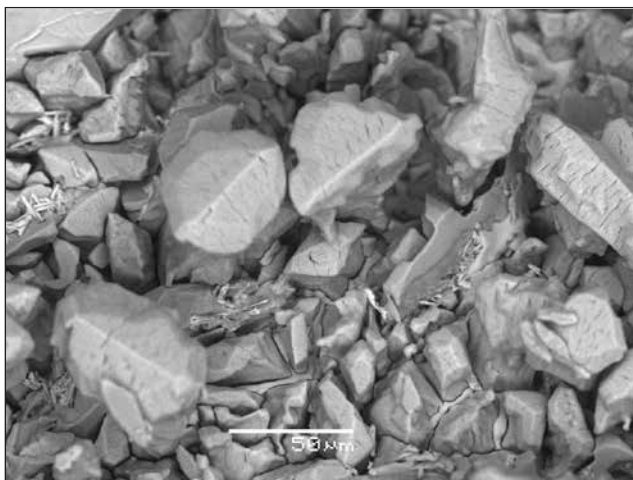

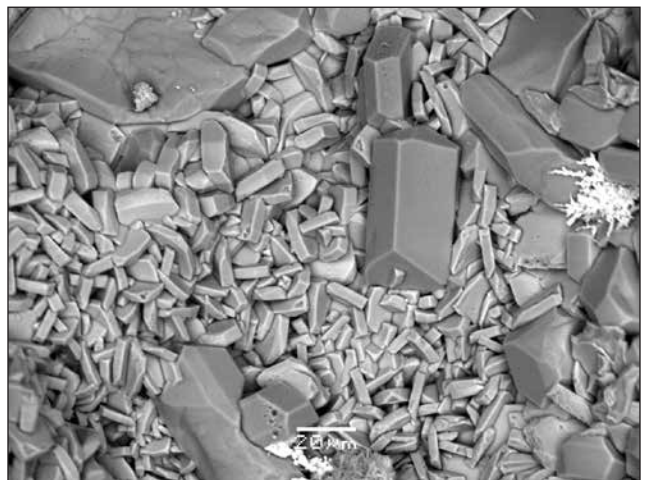Figure 9. Equant boussingaultite crystals with tabular gypsum. SEM image.

Figure 10. Boussingaultite (larger medium gray) with bloedite (small light gray) crystals. SEM image.

4 mm) have been found in unconsolidated material below other crusts at F1 (Figures 9, 10).

Tschermigite $(NH_4)Al(SO_4)_2 \cdot 12H_2O$

XRD analyses have indicated that minor amounts of tschermigite occur with boussingaultite and gypsum in samples from F1 and F2. It has not been recognized in hand specimens.

Sal ammoniac NH_4Cl

Minor amounts of sal ammoniac have been identified with mascagnite by EDS from F2 (Figure 7). It also occurs in evaporation residues of water collected from hot milky pools at F2. It has not been recognized in hand specimens. Sal ammoniac specimens from the fumaroles were identified as early as 1850, by the less than scientific method of "the sharpness of their taste" (Leconte, 1855).

Epsomite $MgSO_4 \cdot 7H_2O$

Epsomite was a major constituent of a small light gray ring around a 1 m orange patch of boussingaultite at F1.

Tamarugite $NaAl(SO_4)_2 \cdot 6H_2O$

Tamarugite was identified by XRD from one specimen with alum-(Na) in a sulfate patch at the SE end of F2 that also contained lecontite, mascagnite and boussingaultite. It has not been recognized in hand samples.

Bloedite $Na_2Mg(SO_4)_2 \cdot 4H_2O$

An FTIR survey of a small gryphon dubbed "Sulfur Hill" on the southwest side of F2 indicated the presence of bloedite. It was found in localized areas of two roughly circular (2–3 m dia.) white sulfate deposits associated with small vents at ground level. It also has been identified by XRD from several areas at F2 where it is associated with boussingaultite (Figure 10). In January 2014 extensive regions of halite at the perimeter F1 were found to contain minor amounts of thenardite and bloedite.

Konyaite $Na_2Mg(SO_4)_2 \cdot 5H_2O$

On November 28, 2013 botryoidal efflorescent konyaite occurred in growths collected from several inch-deep boot prints following a heavy rain that occurred 5 days earlier. On a later trip it formed more extensive deposits at the base of a small gryphon (Sulfur Hill at F2). Konyaite is relatively unstable and under low humidity conditions alters to bloedite (van Doesburg, et al., 1982).

Thenardite $NaSO_4$

The presence of thenardite appears to be ephemeral. Crystalline growths of thenardite up 1.5 cm have been observed with mirabilite scattered on mud flats near the brush line southeast of the F2 fumarole field. Isolated patches of thenardite have also been identified from the outer portions of the F2 north complex. About a month after a heavy rain (0.94") on November 23, 2013 extensive crusts of thenardite, often with or after mirabilite (Figure 11) were observed on the west side of F2 complex and the F2 SE brush line mud flats. These crusts were not present on previous visits. In January 2014 extensive regions of halite around F1 were identified as containing minor amounts of thenardite and bloedite.

Mirabilite $NaSO_4 \cdot 10H_2O$

The existence of mirabilite is also ephemeral and extensive crusts altering to thenardite were observed in late December 2013 on the west side of the F2 field and along the brush line SE of F2. Bladed crystals of mirabilite, to 4 mm x 20 mm, altering to thenardite were found in deep boot prints and tire tracks at F2. At some point after the visit on November 29, 2013 these depressions evidently partially filled with saturated fluids from which the mirabilite crystallized. The thenardite forms pseudomorphic hollow casts after the mirabilite crystals.

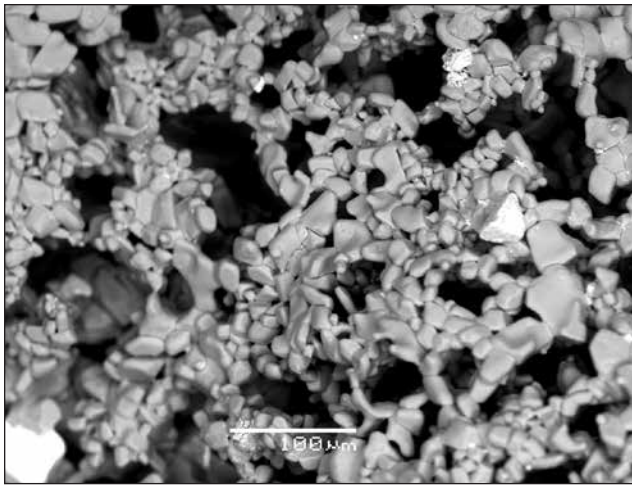Figure 11. Thenardite casts after mirabilite crystals. F2 fumarole field.

Figure 12. Lattice work of minute nitratine crystals. Sulfur Hill gryphon – F2 fumarole field. SEM image.

Nitratine $NaNO_3$

Nitratine was originally identified during an FTIR field survey of a small gryphon dubbed "Sulfur Hill" on the southwest side of F2. It occurs as delicate branching intergrowths of white to clear 0.05 mm crystals (Figure 12). In January 2014 an FTIR survey of sulfate patches in the SE corner of F2 revealed the presence of nitratine. It was inconspicuous and found in black and brown areas just outside of the ammonium sulfate growths around small bubbling pools and vents. On the same trip areas several meters across at F1 were found by FTIR to contain nitratine. Many of these areas were also black to brown in color like at F2, however, thin white crystalline crusts of nitratine were also common. Nitratine had been identified as early as 1902 from along the old beach lines of the Salton Sea east of the "Mud Volcanoes" in T.10S., R.14E. (Bailey, 1902).

Halite NaCl

Halite is ubiquitous as thin white surface films and crystalline crusts away from the gryphons and fumaroles. The extent of the halite efflorescence varies depending how recently it rained and the amount of time to draw saline solutions to the surface from capillary action. Cubic crystals of halite to 3 mm have been observed in boot prints and tire tracks after heavy rains.

Lynch, et al (2013) identified 9 sulfate minerals occurring at the fumarole fields, which have continued to change with time since they emerged from the Salton Sea in about 2007 as a result of falling sea/lake levels. This study has increased the number of identified sulfate and evaporite minerals to 15 which should greatly aid in making more accurate remote sensing mineral distribution maps. A number of LWIR remote sensing data collects have been made since 2009, in addition to those reported by Tratt, et al. (2011). This affords the possibility of plotting the development and evolution of the sulfate deposits as a function of time since emergence of the fumaroles and various rainfall conditions.

Davis–Schrimpf Fumarole Field mineralogy

The Davis–Schrimpf (D–S) fumarole field is located at the northeast corner of Davis (now Wister) and Schrimpf roads 4 miles SW of Niland. It is on property leased to Energy Source from whom permission to enter must be obtained. It has been studied in detail by Onderdonk et al., (2011). It differs from the F1–F2 fields in that the temperatures are lower (to 69C) and the mud somewhat cooler and thicker. Many mud pots are present and the gryphons are typically taller (to 2 m) than at F2 and are often hollow. Bursting mud bubbles can be heard reverberating in the gryphons even though no activity is visible on the outside. Other than thin halite crusts at ground level, "salt" accumulations are uncommon at D–S. The only interesting sulfate occurrences
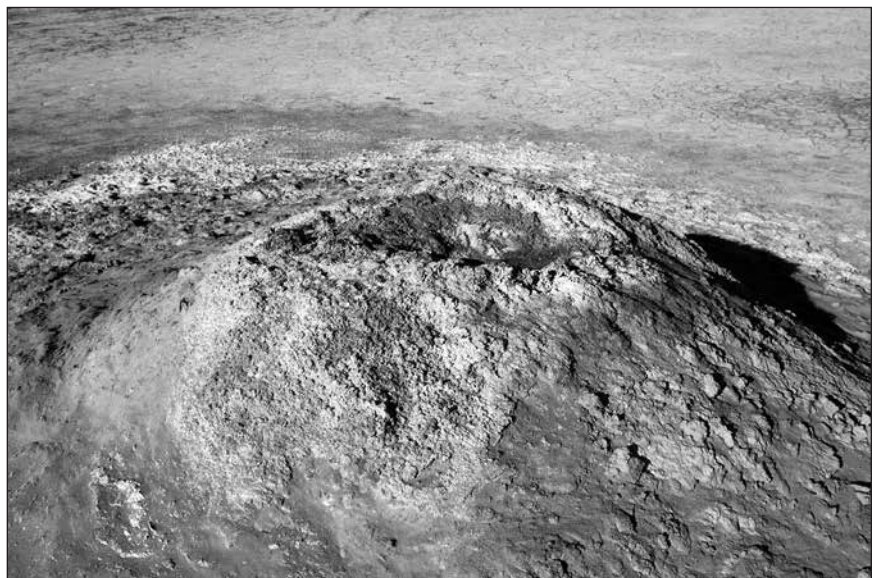

Figure 13 . Sulfate mineralization is concentrated at the summit of gryphon S3 (FOV ~ 2 m). Davis-Schrimpf fumarole field.
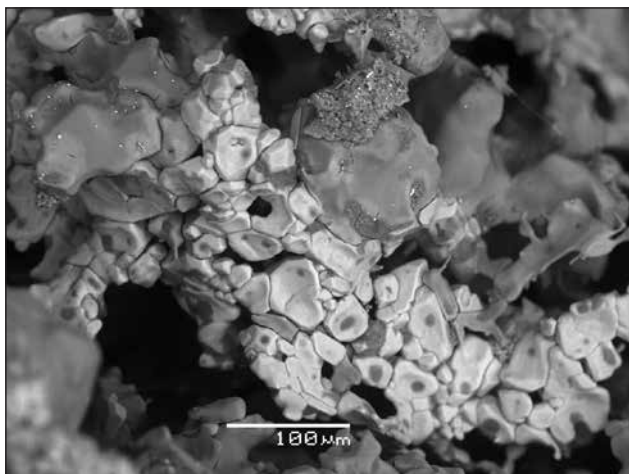
Figure 14. Alum-(K) (medium gray) and Fe sulfate (light gray) from Davis-Schrimpf S3 gryphon. SEM image.

Figure 15. Hexahydrite from Davis-Schrimpf S3 gryphon. SEM image.

are located at the south end of the field (Mazzini, et al., 2011). They consist of two white to light yellow patches (S1: 1 x 1.5 m and S2: 3 x 3 m) at ground level and two small episodic gryphons (S3, S4) approximately 1 m high. S2 and S4 are the eastern most features. The S1 and S2 sulfate patches are nominally at ambient temperature while the gryphons S3 and S4 have elevated temperatures (to 37C) at their summit vents. During visits in November and December 2013 the vent on S4 was dry and could be heard hissing. Subsequent to December 21, 2013 and before January 17, 2014 a mud eruption(s?) occurred producing several flows to 2 meters in length. During the January 2014 visit S4 could be heard loudly gurgling. The majority of the sulfates are concentrated at S2 and S3. Only S3 was sampled during our first two visits. At those times the sulfates at S3 were located at the top of the gryphon, in an area approximately 35 cm in diameter that surrounded the central vent (Figure 13). They consisted of delicate white to yellow lattice works consisting of hexahydrite and tamarugite. Following a heavy rain on November 23, 2013 the sulfates had been dispersed down the sides of the gryphon. By January 2014 the delicate sulfate crusts at the top of S3 had regrown. Tamarugite, bloedite, gypsum and K-ferrite had been reported previously from D–S (Mazzini, et al, 2011).

Alum-(K) KAl$(SO_4)_2 \cdot 12H_2O$
Alum-(K) is a relatively common constituent with bloedite and gypsum at S2 and gypsum at S3. It occurs as crude minute (0.1 mm) octahedral crystals with Fe-sulfates (Figure 14).
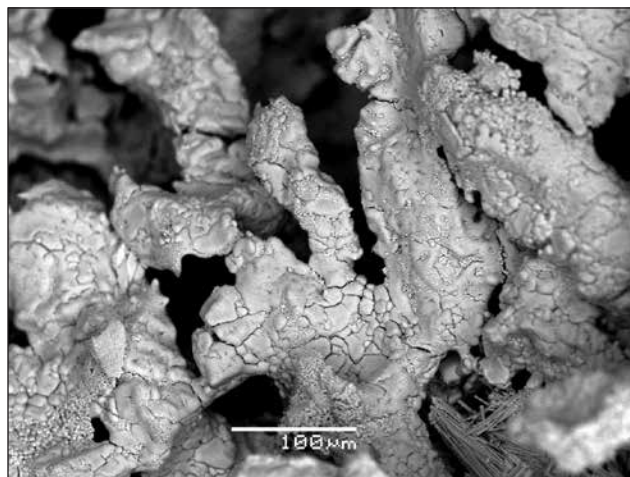
Bloedite Na$_2$Mg$(SO_4)_2 \cdot 4H_2O$
Bloedite was identified by XRD and EDS with thenardite and gypsum in chalky white patches from S1 and S2 and in minor amounts near the vent on S4.

Epsomite MgSO$_4 \cdot 7H_2O$
Hexahydrite MgSO$_4 \cdot 6H_2O$
Starkeyite MgSO$_4 \cdot 4H_2O$
Very fine grained (<0.03 mm) hexahydrite is relatively common at S3 and S2 where it occurs with tamarugite and gypsum (Figure 15). Epsomite and starkeyite have been identified by XRD from isolated samples from S3. It would not be surprising to also find pentahydrite (MgSO$_4 \cdot 5H_2O$) present at some point in time.

Gypsum CaSO$_4 \cdot 2H_2O$
Anhydrite CaSO$_4$
Gypsum has been identified in material beneath many of the delicate sulfate growths at the top of S3 and at S1, S2 and S4. It was also identified in the subsurface soil at S1–S2 (Mazzini,et al., 2011).

Halotrichite Fe^{2+}Al$_2(SO_4)_4 \cdot 22H_2O$
Pickeringite MgAl$_2(SO_4)_4 \cdot 22H_2O$
Silky white fibrous pickeringite-halotrichite has been found at S3 associated with tamarugite, voltaite, hexahydrite, starkeyite and gypsum (Figure 16). Visually it is indistinguishable from tamarugite.

Natrojarosite NaFe$_3(SO_4)_2(OH)_6$
Thin yellow crusts of minute (0.010 mm) pseudo-hexagonal crystals on S3 have a composition, determined by semiquantitative EDS, to be similar to natrojarosite. It is associated with hexahydrite and Fe-pickeringite

Figure 16. Acicular Fe-pickeringite from Davis-Schrimpf S3 gryphon. SEM image.
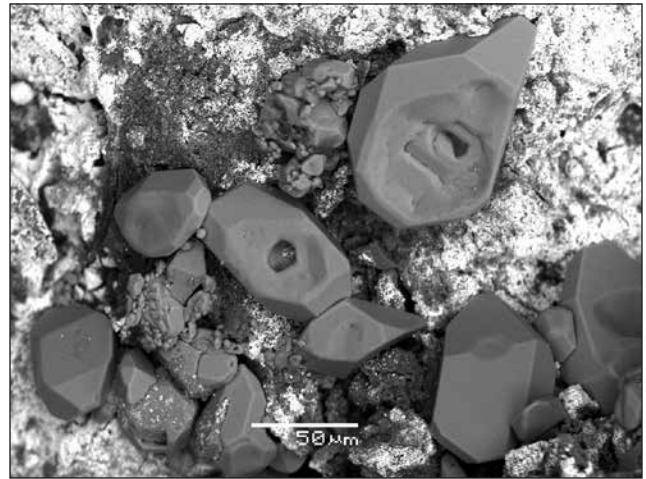

Figure 17 . Cavernous sulfur crystals and cinnabar (white) from Davis-Schrimpf gryphon S3. SEM image.

Figure 18. Fibrous tamarugite crystals (FOV = 3 mm). Davis-Schrimpf gryphon S3.
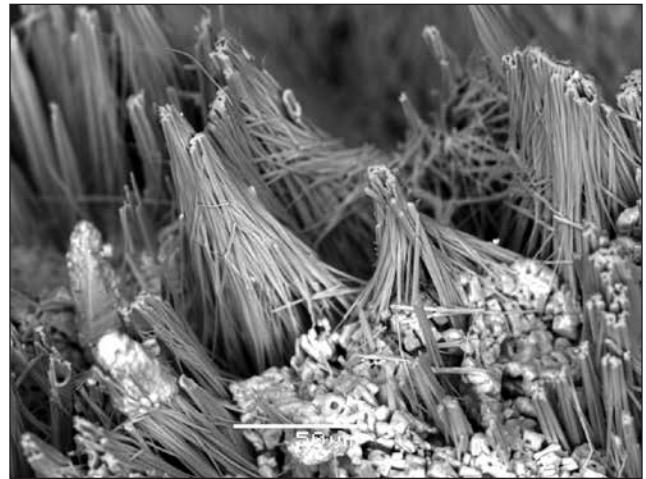

Figure 19. Fibrous tamarugite crystals – SEM image. Davis-Schrimpf gryphon S3.

Sulfur S
Sparse minute (0.05 mm) light yellow equant sulfur crystals were observed near the vent of S4 prior to the mud eruption. Similar sulfur crystals have been found at S3 associated with submicron cinnabar crystals (Figure 17).

Tamarugite $NaAl(SO_4)_2 \cdot 6H_2O$
Tamarugite was found as white to cream-colored, often twisted and tapered, silky fibrous growths to 2 mm in length associated with hexahydrite on S3 (Figures 18, 19).

Thenardite $NaSO_4$
Thenardite was identified by XRD and EDS with bloedite in chalky white patches from S1 and S2. It has also been found in minor amounts of the flank and base of S3 after a heavy rain.

Voltaite $K_2Fe_5^{2+}Fe_3^{3+}Al(SO_4)_{12} \cdot 18H_2O$
Microcrystalline crusts of voltaite have been found on S3 associated with Fe-pickeringite and tamarugite (Figure 20).

Figure 20. Voltaite on acicular Fe-pickeringite from Davis-Schrimpf S3 gryphon. SEM image.

Figure 21. Magnesium carbonate mineralization around a salse. Large salse is ~3 m wide. Rt 111 cold mound springs. Note smaller salses and cracked pressure ridges.

From a remote sensing standpoint, the sulfate deposits at the Davis–Schrimpf fumarole field are near, or below, the spatial resolution (1m x 1 m) of the SEBASS/Mako sensor. This combined with the fact that they are mixtures implies that individual mineral identifications may not be possible. A LWIR remote sensing study of the D–S field has been published (Reath and Ramsey, 2013). They mapped the small sulfate bodies described above as containing quartz with minor amounts of anhydrite but did map extensive areas of a tentative unidentified Mg-sulfate mineral and anhydrite around the

fumarole area. Reath and Ramsey performed very limited and inconclusive ground truth sampling and analyses to support their conclusions and their maps have gross georeferencing errors (N arrow is actually W and figures are mirror images). The work of Mazzini et al.(2011) and this work failed to identify any significant anhydrite or Mg-sulfate minerals away from the very localized areas described above.

CA Route 111 Mound Springs Mineralogy

A field of low mound springs is located on private property just east of California Route 111 at Wister Road, 5 miles NW of Niland. These springs were noted (W9 and W10) by Lynch and Hudnut (2008) in their study of the nearby Wister mud pot lineaments, but they are outliers and have a significantly different structure. Mound springs are cold gryphons with central pools (salses). At these mound springs the fluid is very watery with only minor carbon dioxide bubbling and turbulence. As a result, the springs form volcanoes that are of "shield" type, up to 25 m in diameter, with very low relief. Central pools range from 15 cm to 4 m and the pH is nominally neutral
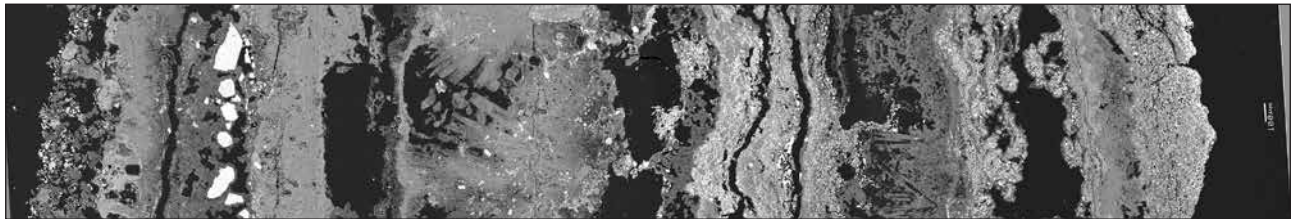

Figure 22 (above). SEM image of polished cross section through a magnesium carbonate deposit from Rt 111 cold mound spring. Scale bar at right is 100 μm; total FOV = 6.2 mm. Outside surface is at left. Black areas are voids and bright white spots are clastic quartz and feldspar grains. Medium gray bands are predominantly magnesium carbonates, while light gray bands contain some fine grained aragonite. At left of center and middle right are voids with fine grained magnesium carbonates replacing bladed crystals of an unknown mineral.

Figure 23 (right). SEM image of polished cross section through a magnesium carbonate deposit from Rt 111 cold mound spring. Large angular grains are clastic quartz and feldspar (white elongate grains near scale bar are mica). Areas with minute light grains (top left) contain aragonite.
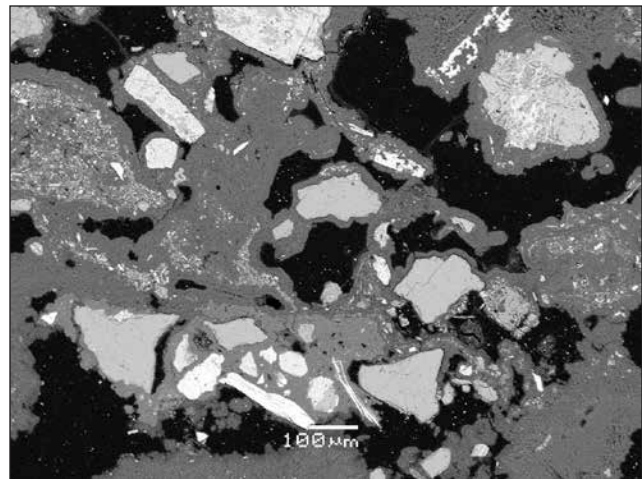
(6.5–7.5). The total dissolved solids content of three pools is 2.0 % with the dominant residue after evaporation being halite with trace amounts of carbonates such as dolomite and magnesite also being present. White crusts of magnesium carbonates (magnesite, hyromagnesite and nesquehonite), in addition to aragonite, dolomite and northupite, are associated with some of the salses in the northeast corner of the field (Figure 21). The carbonate deposits are bedded with significant porosity or gaps between relatively solid layers (Figures 22, 23). Individual layers may be 1) relatively pure fine grained magnesium carbonates, 2) magnesium carbonates mixed with fine grained (< 10 μm) acicular aragonite, or 3) contain significant amounts of clastic grains (quartz, plagioclase, potassium feldspar, mica (to 150 μm) in a matrix of magnesium carbonates (Figure 23). The clastic grains may represent windblown sand that was subsequently cemented by carbonates. The presence of halite with the magnesium carbonate deposits is ephemeral. At some times it is nearly absent, while at others it may form a near continuous layer to about 2–3 mm thick. This ephemeral halite may be responsible for the large gaps between the carbonate layers. Conceivably a layer of the carbonate may form on halite, which subsequently dissolves to form the large gaps.

Aragonite CaCO$_3$
Strontianite SrCO$_3$
Aragonite occurs as minute acicular crystals (to 0.01 mm) that tend to be concentrated in specific layers in the magnesium carbonate deposits (Figure 24). Calcium-rich strontianite is uncommon and has been found with strontian-barite in coarse grained (to 0.07
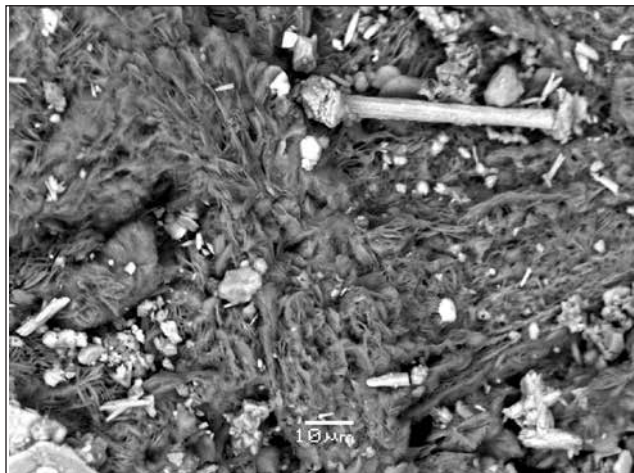
mm) aragonite, dolomite and magnesite veins in fine grained banded dolomite–aragonite nodules.

Dolomite CaMg(CO$_3$)$_2$
Dolomite is a major constituent of some surface crusts near a salse in the NE corner of the field and in some layered nodular growths.

Halite NaCl
Extensive halite efflorescence is common in the southwest corner of the field and in other areas is ephemeral. In some areas along the northern margin of the field twisted filiform growths consisting of stacked halite crystals were observed (Figures 25, 26). This type of halite growth is uncommon but has been observed in some caves where air flow has been considered critical to their formation (Filippi, et al., 2011).
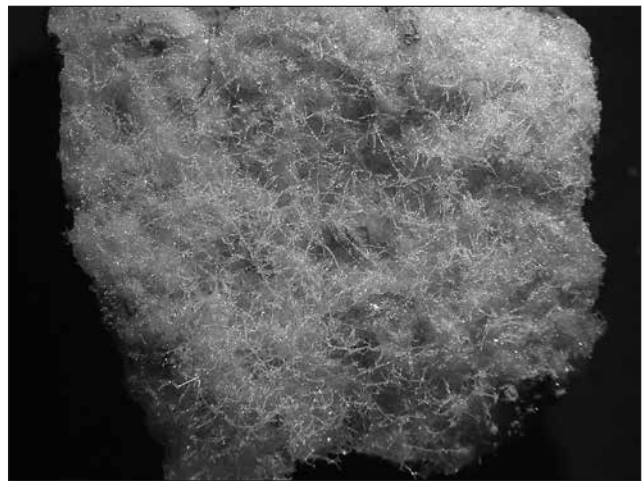

Figure 25. Filiform halite crystal growth (3 cm x 3 cm). Rt 111 mound springs.

Figure 24. Platy hydromagnesite crystals (gray) with acicular aragonite (white). Rt 111 mound springs. SEM image.
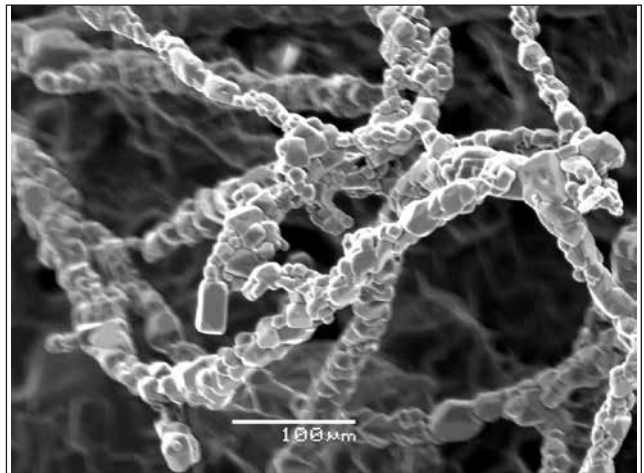

Figure 26. Filiform halite crystal growth. Rt 111 mound springs. SEM image.
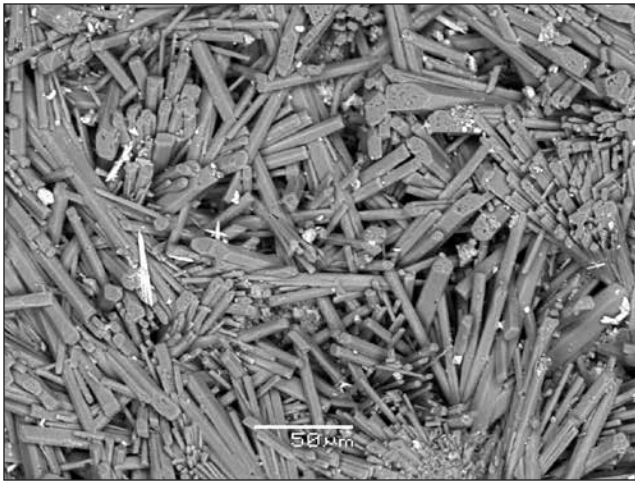
Figure 27. Acicular nesquehonite crystals from Rt 111 mound springs. SEM image.

Figure 28. Octahedral northupite crystals with halite (white). Rt 111 mound springs. SEM image.

Hydromagnesite $Mg_5(CO_3)_4(OH)_2 \cdot 4H_2O$

Hydromagnesite forms dense aggregates of tiny (0.01 x 0.001 mm) platelets, often associated with aragonite (Figure 24) in crusts with other magnesium carbonates.

Magnesite $MgCO_3$

Fine grained white to light gray magnesite is common as surface crusts and bulk deposits in the northeast corner of the field.

Nesquehonite $Mg(HCO_3)(OH) \cdot 2H_2O$

Nesquehonite is found as small (0.1 x 0.01 mm) acicular crystals forming white mats on the surface surrounding some salses (Figure 27).

Northupite $Na_3Mg(CO_3)_2Cl$

Minute (0.10 mm) octahedra of northupite form white crusts with other magnesium carbonates around some salses in the northeast corner of the field (Figure 28).

Polyhalite $K_2Ca_2Mg(SO_4)_4 \cdot 2H_2O$

Polyhalite and another potassium sulfate were identified by XRD and EDS as occurring with hydromagnesite, halite and aragonite near some small active gryphons.

Thenardite $NaSO_4$

Thenardite is uncommon and with the exception of rare barite the only sulfate found at the RT 111 deposit. It was found as clusters of minute (0.01 mm) tabular crystals associated with halite, aragonite and hydromagnesite near a small active gryphon.

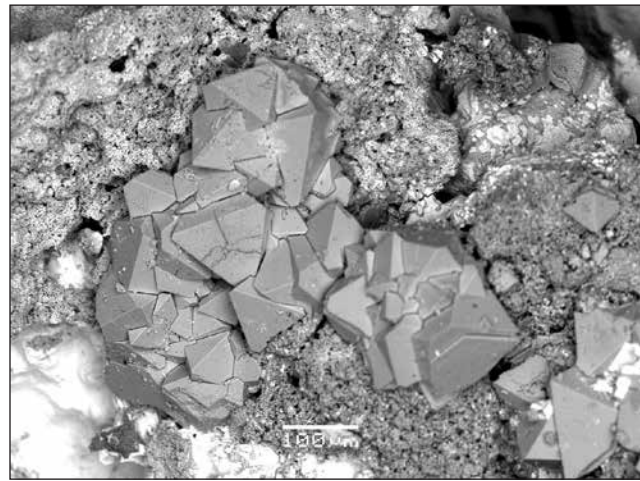The Rt 111 mound spring deposits are unusual in that many magnesium carbonate deposits are associated with the weathering of ultramafic rocks (Braithwaite and Zedef, 1996; Renaut and Stead, 1991). The source of the magnesium in the Rt 111 deposits is uncertain. From our SEM studies of the RT 111 magnesium carbonate deposits we have shown that some minerals (northupite, nesquehonite) occur as crystals in excess of 10s of microns which should produce strong LWIR reflectance spectra, which has been confirmed with our field FTIR (Exoscan) measurements. Hydromagnesite and to a lesser extent aragonite are found as crystals < 10 microns which produce very weak and low contrast LWIR reflectance signatures. In fact, in the field, the Exoscan did not have sufficient signal from hydromagnesite samples to acquire spectra. This could only be accomplished in the laboratory with a high sensitivity mercury cadmium telluride detector.

White Rock is a feature on Mars that gathered a significant amount of attention during the 1990s (Russell et al., 1999) and was suspected of containing magnesium carbonates, which would have confirmed the presence of water, making White Rock a possible target for the search of past life on Mars. On earth some magnesium carbonate spring and lake deposits have been linked to biologic activity (Braithwaite, et al., 1996; Russell et al., 1999; Power, et al., 2007). LWIR remote sensing using TES on the Mars Global Surveyor spacecraft failed to confirm the presence of carbonates and albedo measurements argued against their existence (Ruff, et al., 2001). In fact, TES failed to produce any LWIR spectra signature from White Rock so the presence of carbonates cannot be completely ruled out. Our studies have shown that

very fine grained hydromagnesite can produce very weak, near featureless LWIR reflectance spectra, potentially analogous to what has been seen on Mars for White Rock. This situation is similar to what we have observed for calcium carbonate rocks with very fine scale weathering surfaces (Kirkland, et al., 2002 and 2003). The RT 111 magnesium carbonate deposit is an easily accessible site that could be used to study the role of carbonate mineral particle size on detectability by various remote sensing platforms, which might be used to better understand the limitations of LWIR studies on Mars and on earth.

Acknowledgements

References

Anthony, J. W., Bideaux, R. A., Bladh, K. W. and Nichols, M. C. (2003) Handbook of Mineralogy, Volume V, Borates, Carbonates, Sulfates, p82.

Bailey. G. E. (1902) The saline deposits of California, Calif. State Min. Bur. Rpt. 24, pp. 178, 180.

Braithwaite C. J. R. and Zedef, V. (1996) Hydromagnesite stromatolites in an alkaline lake, Salda Golu, Turkey, J. Sediment. Res., 66, 991-1002.

Dunning, G. E. and Cooper, J. F., Jr. (1993) History and minerals of the Geysers, Sonoma County, California, Mineralogical Record, 24, 339-354.

Filippi, M., Bruthans, J., Palatinus, L., Zare, M. and Asadi, N. (2011) Secondary halite deposits in the Iranian salt karst: general description and origin, Int. J. Speleology, 40, 141-162.

Hackwell, J. A., D. W. Warren, R.P. Bongiovi, S. J. Hansel, T. L. Hayhurst, D. J. Mabry, M. G. Sivjee, and J. W. Skinner (1996), "LWIR/MWIR imaging hyperspectral sensor for airborne and ground-based remote sensing," Proceedings of SPIE, 2819, 102-107, doi:10.1117/12.258057.

Hanks, H.G., (1882). Mud volcanoes and the Colorado Desert. Second Report of the State Mineralogist of California; From December 1, 1880 to October 1, 1882, Calif. Min. Bur. Rept., 2, 227-240.

Kirkland, L., Herr, K., Keim, E., Adams, P., Salisbury, J., Hackwell, J. and Treiman, A. (2002), First use of an airborne thermal infrared hyperspectral scanner for compositional mapping, Remote Sens. Environ., 80, 447-459.

Koenig, J. B., (1969) The Geysers geothermal field, Mineral Information Service, 22, 123-128.

Leconte, (1855) Account of some volcanic springs in the desert of the Colorado, Southern California, Am. J. Sci. 2nd ed., 19, 1-6.

Lynch, D. K and Hudnut, K. W. (2008) The Wister mud pot lineament: Southeastward extension or abandoned strand of the San Andreas fault, Bull. Seismol. Soc. Amer., 98, 1720-1729.

Lynch, D. K., Hudnut, K. W. and Adams, P. M. (2013) Development and growth of recently-exposed fumarole fields near Mullet Island, Imperial County, California, Geomorphology, 195, 27-44.

Mazzini, A., Svenson, H., Etiope, G., Onderdonk, N. and Banks, D. (2011) Fluid origin, gas fluxes and plumbing system in the sediment-hosted Salton Sea geothermal system (California, USA), J. Volcano. Geotherm. Res., 205, 67-83.

McKibben, M. A. (2008) The Salton Sea geothermal brines, 2008 Desert Symposium Field Guide and Proceedings, Cal. State Univ., Fullerton Desert Studies Consortium, 102-106.

Onderdonk, N., Shafer, L, Mazzini, A. and Svenson, H. (2011) Controls on the expression and evolution of gryphons, mud pots, and caldera features at hydrothermal seeps in the Salton Sea Geothermal Field, Southern California, Geomorphology, 130, 327-342.

Pemberton, H. E (1983) Minerals of California, Van Nostrand Reinhold, New York, 591pp.

Ross, C. P. and Yates, R. G. (1942) The Coso quicksilver district Inyo County, California, U.S.G.S. Bull. 936-Q, 394-415.

Power, I. M., Wilson, S. A., Thom, J. M., Dipple, G. M. and Southam, G. (2007) Biologically induced mineralization of dypingite by cyanobacteria from an alkaline wetland near Atlin, British Columbia, Canada, Geochemical Transactions, 8:13, doi:10.1186/1467-4866-8-13.

Reath, K. A. and Ramsey, M. S. (2013) Exploration of geothermal systems using hyperspectral thermal infrared remote sensing, J. Volcan. Geotherm. Res., 265, 27-38.

Renaut, R. W. and Stead, D. (1991) Recent magnesite-hydromagnesite sedimentation in playa basins of the Cariboo plateau, British Columbia, British Columbia Geol. Soc. Geol. Fieldwork 1990, Paper 1991-1.

Ruff, S. W., Christensen, P. R., Clark, R. H., Kieffer, H. H., Malin, M. C., Bandfield, J. C., Jackosky, B. M., Lane, M. D., Mellon, M. T. and Presley, M. M. (2001) Mars' "White Rock" feature lacks evidence of an aqueous origin: Results from Mars Global Surveyor, J. Geophys. Res., 106, 23921-23927.

Russell, M. J., Ingham, K., Zedef, V., Maktav, D., Sunar, F., Hall, A. J. and Fallick (1999) Search for signs of ancient life on Mars: expectations from hydromagnesite microbalites, Salda Lake, Turkey, J. Geol. Soc., London, 156, 869-888.

Tratt, D. M., Young, S. J., Lynch, D. K., Buckland, K. N., Johnson, P. D., Hall, J. L., Westberg, K. R., Polak, M. L., Kasper, B. P. and J. Qian (2011), "Remotely-sensed ammonia emission from fumarolic vents associated with a hydrothermally active fault in the Salton Sea Geothermal Field, California," J. Geophys. Res., 116(D21), D21308, doi:10.1029/2011JD016282.

Warren, D. W., Boucher, R. H., Gutierrez, D. J., Keim, E. R. and M. G. Sivjee (2010), "MAKO: A high-performance, airborne imaging spectrometer for the long-wave infrared," Proceedings of SPIE, 7812, 78120N, doi:10.1117/12.861374.

Van Doesburg, J. D. J., Vergouen, L. and van der Plas, L. (1982) Konyaite $Na_2Mg(SO_4)_2 \cdot 5H_2O$, a new mineral from the Great Konya Basin, Turkey, Am. Mineral., 67, 1035-1038.